Contribution from the Department of Chemistry,
Massachusetts Institute of Technology, Cambridge, Massachusetts 02139

Electronic Absorption Spectrum of Chromous Acetate Dihydrate and Related Binuclear Chromous Carboxylates

STEVEN F. RICE, RANDALL B. WILSON, and EDWARD I. SOLOMON*

Received March 26, 1980

Low-temperature polarized single-crystal absorption spectral data on $Cr_2(CH_3CO_2)_4(H_2O)_2$ and survey spectral data on a series of $Cr_2(RCO_2)_4L_2$ analogues are reported. In addition, high-resolution data are presented on new weak features which appear at low temperature in the absorption spectrum of $Cr_2(CH_3CO_2)_4(H_2O)_2$ and which correspond to additional electronic transitions. The polarized absorption data are interpreted in terms of molecule-oriented transition moments which allow a determination of the symmetry of the two dominant spectral features at ~21 000 and ~30 000 cm^{-1} as $^1E_g \leftarrow {}^1A_{1g}$ and $^1E_u \leftarrow {}^1A_{1g}$ transitions, respectively, in D_{4h}. These features can be further associated with specific excited states ($\delta \rightarrow \pi^*$ and $n p_\pi \rightarrow \pi^*$, respectively) through a band shape analysis approach combined with the chemical perturbation of variation in Cr–Cr distance. Finally, the ground state Cr–Cr stretching frequency is estimated from excited-state vibronic analysis to be in the 150–250-cm^{-1} range.

Introduction

The electronic structure of carboxylate-bridged binuclear complexes has been of considerable interest for many years and has been the subject of numerous theoretical[1] and experimental[2] studies. One of the earliest representations of this class of molecules is $Cu_2(CH_3CO_2)_4(H_2O)_2$. This molecule exhibits many unusual experimentally accessible features such as its magnetic[2a] and optical properties[2b] that have been associated with its binuclear structure. More recently, interest has centered on the Mo and Cr analogues (and derivatives), and several molecular orbital[1c-e] and spectral[2d,e,3] studies of these systems have appeared. Although there has been disagreement as to the nature of the bonding in the $Cr_2(RCO_2)_4L_2$ systems, the recent work of Cotton et al.[4] on the determination of Cr–Cr bond lengths in a large number of $Cr_2(RCO_2)_4L_2$ species and the application[1e] of the SCF–Xα molecular orbital method support the existence of a quadruple bond in the ground states of these molecules. This unique type of bond is the result of overlap of the z^2 (σ), xz, yz (π), and xy (δ) orbitals between the two chromium centers. Much less is known about the excited states of the binuclear chromous carboxylates. Spectral assignments[3] have mainly been concerned with general spectroscopic observations and comparisons to the $Cu_2(CH_3CO_2)_4(H_2O)_2$ spectrum; however, this compound is more reasonably treated in terms of a weak interaction approach (a coupled chromophore model).[1f] In the present study, we report low-temperature polarized single-crystal absorption data for $Cr_2(CH_3CO_2)_4(H_2O)_2$ and survey spectral data on a series of $Cr_2(RCO_2)_4L_2$ analogues. In addition, high-resolution data are presented on new sharp, weak features which appear at low temperature in the absorption spectrum of $Cr_2(CH_3CO_2)_4(H_2O)_2$ and which correspond to additional electronic transitions.

The polarized absorption data are interpreted in terms of molecule-oriented transition moments which allow a determination of the symmetry of the two dominant spectral features. These features can further be associated with specific excited states through a band shape analysis approach combined with the chemical perturbation of variation in Cr–Cr distance. These assignments are then discussed along with the newly observed bands.

Experimental Section

$Cr_2(CH_3CO_2)_4(H_2O)_2$ was prepared by the method of Ocone and Block.[5] Single crystals, suitable for optical absorption studies, were grown by slow cooling of a saturated aqueous solution sealed under nitrogen. This procedure reproducibly yielded diamond-shaped tabular crystals, the most prominent face displaying an acute bisectrix (B_{x_a}) optical figure when viewed under a polarizing microscope. X-ray measurements identified this face as the (10$\bar{1}$) face of the $C2/c$ unit cell.[6] The b crystallographic axis is perpendicular to the optic plane (b is parallel to the optical Y direction). The polarized absorption spectra obtained with light propagating normal to the (10$\bar{1}$) face (propagation vector **k** parallel to the optical Z direction) and with the electric vector $\parallel$ and $\perp$ to the b axis are designated as π and σ_1, respectively. A third polarization could be obtained by polishing new faces on a thick crystal such that light could propagate along the dielectric axis 90° (about b) away from the previous direction (propagation vector **k** parallel to the optical X direction). Polarized absorption spectra obtained in this way with the electric vector $\perp$ to b are designated as σ_2.

The remaining $Cr_2(RCO_2)_4L_2$ used in this study were prepared by the methods described by Cotton et al.[4] Unpolarized low-temperature absorption spectra of these compounds were obtained from Nujol mulls between quartz disks. The absorption spectrometer and cryogenic system used for these measurements have been previously described.[7]

Results and Interpretation

The π, σ_1, and σ_2 polarized absorption spectra of $Cr_2(CH_3CO_2)_4(H_2O)_2$ at 6 K are shown in Figure 1. There are two major features in these spectra in the regions of 21 000 and 30 000 cm^{-1} which are designated as band I and band II, respectively.

The $C2/c$ unit cell of $Cr_2(CH_3CO_2)_4(H_2O)_2$ has four symmetry-related binuclear molecules per unit cell which lie at sites having rigorous $\bar{1}$ symmetry and have approximate D_{4h} molecular symmetry. For interpretation of the π, σ_1, and σ_2

(1) (a) L. S. Forster and C. J. Ballhausen, *Acta Chem. Scand.*, **16**, 1385 (1962); (b) C. D. Garner, I. H. Hillier, M. F. Guest, J. C. Green, and A. W. Coleman, *Chem. Phys. Lett.*, **41**, 91 (1976); (c) M. Benard and A. Veillard, *Nouv. J. Chim.*, **1**, 97 (1977); (d) J. G. Norman, Jr., H. J. Kolari, H. B. Gray, and W. C. Trogler, *Inorg. Chem.*, **16**, 987 (1977); (e) F. A. Cotton and G. G. Stanley, *ibid.*, **16**, 2668 (1977); (f) A. E. Hansen and C. J. Ballhausen, *Trans. Faraday Soc.*, **61**, 631 (1965).
(2) (a) B. Bleaney and K. D. Bowers, *Proc. R. Soc. London, Ser. A*, **214**, 451 (1952); (b) L. Dubicki, *Aust. J. Chem.*, **25**, 1141 (1972); (c) W. R. King and C. S. Garner, *J. Chem. Phys.*, **18**, 689 (1950); (d) W. C. Trogler, E. I. Solomon, I. Trajberg, C. J. Ballhausen, and H. B. Gray, *Inorg. Chem.*, **16**, 828 (1977); (e) D. S. Martin, R. A. Newman, and P. E. Fanwick, *ibid.*, **18**, 2511 (1979); (f) B. E. Bursten, F. A. Cotton, A. H. Cowley, B. E. Hanson, M. Lattman, and G. G. Stanley, *J. Am. Chem. Soc.*, **101**, 6244 (1979); (g) M. F. Guest, C. D. Garner, I. H. Hillier, I. B. Walton, *J. Chem. Soc. Faraday Trans. 2*, **74**, 2092 (1978); (h) M. F. Guest, C. D. Garner, I. H. Hillier, A. A. MacDowell, and I. B. Walton, *ibid.*, **75**, 485 (1979).
(3) (a) S. Kida, Y. Nakashima, Y. Morimoto, K. Niimi, and S. Yamada, *Bull. Chem. Soc. Jpn.*, **37**, 549 (1964); (b) L. Dubicki and R. L. Martin, *Inorg. Chem.*, **5**, 2203 (1966).
(4) (a) F. A. Cotton, M. W. Extine, and G. W. Rice, *Inorg. Chem.*, **17**, 176 (1978); (b) F. A. Cotton and G. W. Rice, *ibid.*, **17**, 2004 (1978).
(5) L. R. Ocone and B. P. Block, *Inorg. Synth.*, **8**, 125 (1966).
(6) F. A. Cotton, B. G. DeBoer, M. D. LaPrade, J. R. Pipal, and D. A. Ucko, *Acta Crystallogr., Sect. B*, **B27**, 1664 (1971).
(7) R. B. Wilson and E. I. Solomon, *Inorg. Chem.*, **17**, 1729 (1978).

0020-1669/80/1319-3425$01.00/0

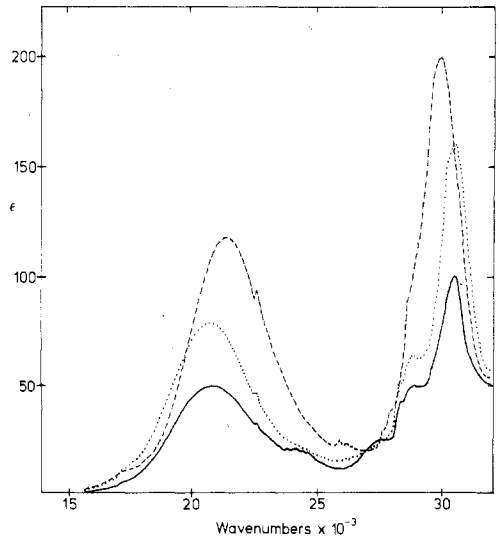

Figure 1. π, σ_1, and σ_2 polarized absorption spectra of $Cr_2(CH_3CO_2)_4(H_2O)_2$ at 6 K: π polarization (dotted curve); σ_1 polarization (dashed curve); σ_2 polarization (solid curve). (Note that ϵ refers to the dimeric molecule.)

polarized absorption spectra, the electric vector of the light must be projected onto a set of molecular axes representing the directions of the transition moment operator for the electronic transitions of the molecule. These molecular axes will be primarily determined by the symmetry of the molecule. The polarization behavior of the π, σ_1, and σ_2 absorption spectra is not consistent with a molecule possessing perfect D_{4h} symmetry (vide infra); therefore, we now consider the highest possible effective symmetry which is consistent with the observed spectra and use this to determine the molecular axes.

The crystal structure[6] shows that the chromous acetate dihydrate molecule has one chromium carboxylate plane (O(1)–Cr–Cr′–O(2)) (denoted as plane 1) with an average chromium–oxygen bond length which is longer by about 0.026 Å than the remaining plane (O(4)–Cr–Cr′–O(3)) (plane 2), where the notation is that of ref 6. If one neglects the axial water molecules, this difference in bond length reduces the approximate D_{4h} molecular symmetry to D_{2h}. This would require the molecular Z axis to be along the Cr–Cr′ direction with the molecular X,Y directions to be contained in planes 1 and 2. The molecular symmetry is further reduced by a deviation of the interplanar O(1)–Cr–O(4) bond angle from 90°. In the absence of the bond length differences, this effect would again reduce the effective symmetry to D_{2h} with Z along the Cr–Cr′ direction, but with the molecular X,Y directions approximately bisecting the O–Cr–O bond angles. The combined effect of these two low-symmetry distortions will be to orient the molecular X,Y axis somewhere in between, the exact orientation being dependent upon the relative effect of the two distortions on the molecular Hamiltonian. One might expect bond length changes to be more important than bond angle changes due to the relative magnitudes of stretching vs. bending frequencies in the vibrational spectrum. Finally, the nonaxiality of the water molecules will tend to shift the molecular Z axis away from the Cr–Cr′ direction.

In principle, it is possible to uniquely determine the direction of the transition moment vector (and molecular axes) in a biaxial crystal by taking polarized absorption measurements along three nonorthogonal propagation directions. However, due to the optical properties of absorbing biaxial crystals, experimental difficulties make this procedure impractical for broad bands. Instead, we use the approach of choosing several reasonable sets of molecular axes and eliminate those inconsistent with the experiment.

Table I. Crystallographic Coordinates for the Polarized Light E Vector and the Molecular Axes

vector	$(a, b, c)^a$
electric (π)	(0, 11.605, 0)
electric (σ_1)	(7.0212, 0, 7.0212)
electric (σ_2)	(4.7627, 0, −3.8920)
molecular **X** (A)	(−2.7067, 9.7460, 1.9893)
molecular **Y** (A)	(7.0961, 0.3658, 6.9520)
molecular **Z** (A)	(3.7815, 6.2895, −3.4868)
molecular **X** (B)	(3.1037, 7.1501, 6.3224)
molecular **Y** (B)	(6.9316, −6.6327, 3.5092)
molecular **Z** (B)	(3.7815, 6.2895, −3.4868)

[a] Multiplied by 10^2.

The transformation between the experimentally obtained π, σ_1, and σ_2 intensities (at a given wavelength) and the intensities one would observe if the electric vector was parallel to the molecular X, Y, or Z axes is given as eq 1 where the

$$\begin{bmatrix} X \\ Y \\ Z \end{bmatrix}_\lambda = \begin{bmatrix} T_{11} & T_{12} & T_{13} \\ T_{21} & T_{22} & T_{23} \\ T_{31} & T_{32} & T_{33} \end{bmatrix} \begin{bmatrix} \pi \\ \sigma_1 \\ \sigma_2 \end{bmatrix}_\lambda = T \begin{bmatrix} \pi \\ \sigma_1 \\ \sigma_2 \end{bmatrix}_\lambda \quad (1)$$

matrix elements of T are determined from the squares of the projections of the electric vector (for each polarization) onto the chosen molecular axes (eq 2).

$$\pi = 0.71X + 0.29Z \qquad \sigma_1 = 1.00Y$$
$$\sigma_2 = 0.29X + 0.71Z \quad (2)$$

Table I gives the normalized vectors (in crystallographic a, b, and c coordinates) for the electric vectors in the π, σ_1, and σ_2 polarizations. In addition, Table I contains the **X**, **Y**, and **Z** molecular axis vectors for $Z\|$ to the Cr–Cr′ axis, $X\perp Z$ and in plane 2, and $Y\perp X,Z$ (orientation A). Also given are the **X**, **Y**, and **Z** molecular axis vectors for $Z\|$ to the Cr–Cr′ axis, $X\perp Z$ and bisecting planes 1 and 2, and $Y\perp X,Z$ (orientation B). These are the limiting orientations for the molecular axes expected from the earlier consideration of the low-symmetry distortions.

We now apply this transformation for the two choices of molecular X, Y, and Z axes to yield the absorption spectra which would be observed with light polarized along these axes. The π, σ_1, and σ_2 spectra were first digitized for input into a computer, and an instrumental base line was carefully subtracted. The digitized data were then transformed point by point by using eq 1. The resulting X, Y, and Z spectra thus obtained were replotted as shown in Figure 2a,b. Figure 2b clearly shows that the molecular axes corresponding to having X and Y bisecting planes 1 and 2 are grossly inappropriate as these predict large negative absorption values. Further investigations along these lines (small rotations of X, Y, and Z from orientation A) indicate that reasonable transformed spectra are obtained only when molecular axes are chosen close (±5°) to orientation A. We therefore proceed by using these as the effective molecular symmetry axes. In Figure 3, the transformed spectra are shown in greater detail. Bands I and II are strong in X and Y yet weak in Z. The small difference in intensity between X and Y as well as the weak Z intensity for these bands may be due to a slight deviation in the actual transition moment vectors from orientation A chosen for the molecular axes. There also may be an intrinsic intensity difference in X and Y from the nonequivalence of these two directions. However, the much greater intensities of the X and Y polarizations as compared to that of Z indicate that bands I and II are predominantly polarized perpendicular to the Cr–Cr′ axis. It should be emphasized that the third polarization, σ_2, clearly demonstrates that there cannot be a Z polarized transition contributing to the low-energy side of band I, as this would lead to a more intense band I in σ_2 polarization which is not the case.

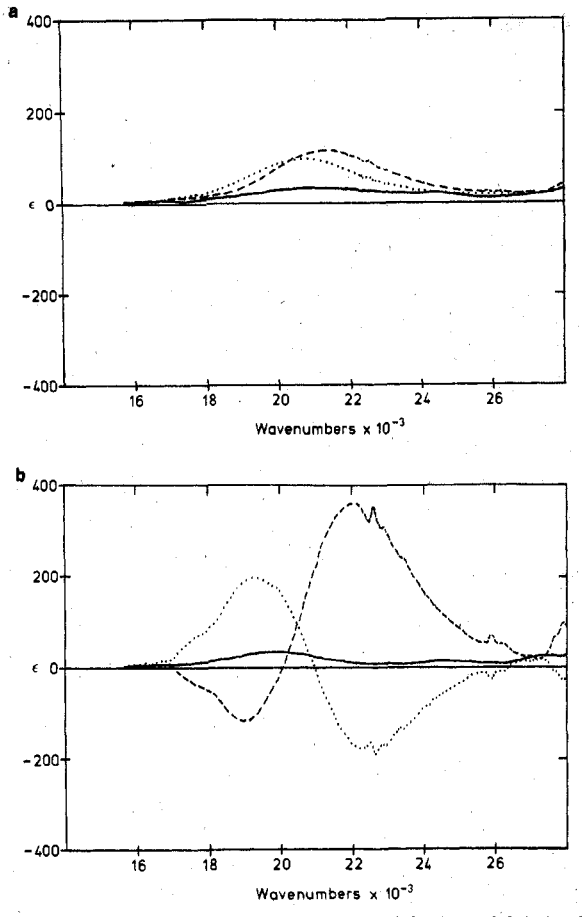

Figure 2. (a) X, Y, and Z polarized spectra of $Cr_2(CH_3CO_2)_4(H_2O)_2$ obtained from eq 1, with use of orientation A for the molecular axes: X polarization (dotted curve); Y polarization (dashed curve); Z polarization (solid curve). (b) X, Y, and Z polarized spectra of $Cr_2(CH_3CO_2)_4(H_2O)_2$ obtained from eq 1, with use of orientation B for the molecular axes: X polarization (dotted curve); Y polarization (dashed curve); Z polarization (solid curve).

Further, the band maxima in the X and Y spectra for both bands I and II are shifted from each other. This X–Y splitting is on the order of 600 cm^{-1} for both bands I and II. A split X,Y polarized transition is only consistent with an excited state which is doubly degenerate in the approximate D_{4h} symmetry of the molecule and splits due to the effects of low symmetry. (A 600-cm^{-1} splitting is also too large to be accounted for by spin–orbit effects in Cr^{2+}, and Jahn–Teller effects would involve the E electronic state coupling to a b_{1g} or b_{2g} vibration in D_{4h}. This is formally equivalent to a T electronic state coupling to an e_g vibration in O_h and thus should not effect the overall band shape or its splitting due to low symmetry.[7]) Thus, we conclude that the orbital symmetry for the states I and II (corresponding to bands I and II) must be of symmetry species E in D_{4h}. The SCF–Xα calculations[1e] on the related anhydrous chromous formate and magnetic susceptibility studies[8] on $Cr_2(CH_3CO_2)_4(H_2O)_2$ indicate that the ground state consists of filled shells. This requires that the doubly degenerate nature of the excited state is the result of electronic promotion either into or out of an $e(D_{4h})$ molecular orbital. The magnitude of the low-symmetry splitting further indicates these $e(D_{4h})$ molecular orbitals involved in the transitions to be metal localized, as these would be the most sensitive to the low-symmetry distortions previously discussed (the crystal structure[6] shows that all carboxylate bond lengths are normal; hence the electronic structure of carboxylate localized orbitals

(8) S. F. Rice and E. I. Solomon, unpublished results.

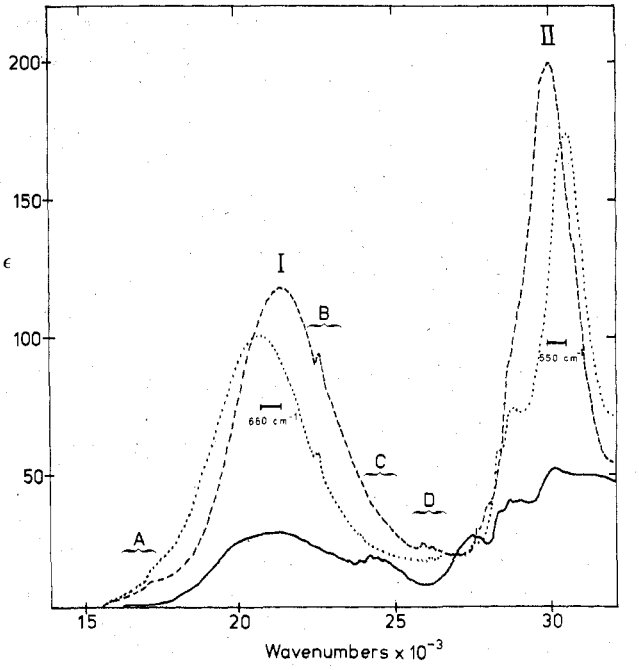

Figure 3. Expanded and labeled X, Y, and Z polarized spectra using orientation A: X (dotted); Y (dashed); Z (solid).

is not expected to be significantly altered in the crystal). Finally, we note the similarity in the low-symmetry splittings of bands I and II, suggesting the possibility that the same $e(D_{4h})$ molecular orbital is involved in both transitions.

We next direct attention to the several sets of weak features found in the absorption spectrum of $Cr_2(CH_3CO_2)_4(H_2O)_2$. Bands A–D are indicated in Figure 3 and expanded in Figure 4a–c. Studies on these bands argue strongly against their being impurities. By varying the crystal thickness, the surface area to volume ratio could be adjusted. Beer's law was obeyed, establishing that surface oxidation is not significant. In addition, the extinction coefficients remained constant for many samples prepared under different reaction and recrystallization conditions. The most likely impurity bands are Cr^{2+} or Cr^{3+} spin-forbidden transitions. However, these bands would be at least an order of magnitude weaker than their associated spin-allowed transitions which are not observed. The lowest energy absorption feature is designated as band A (Figure 4a). Low-temperature absorption measurements from 4000 to 16 000 cm^{-1} using thick crystals revealed only absorption features which could be attributed to ground-state vibrational overtones (or combinations) from the acetate and water groups (from a comparison to data on $Cu_2(CH_3CO_2)_4(H_2O)_2$). Analysis of the band shape of band I, as well as a comparison of the shift in spectral energies for the $Cr_2(RCO_2)_4L_2$ species (vide infra), shows that band A cannot be associated with the electronic or vibronic origins of band I. Deuteration of both the axial waters and carboxylate methyl groups shows that band A is not associated with a ground-state vibration and thus must be a new electronic transition. Band A is predominantly X,Y polarized, with member A_2 appearing to be totally symmetric off A_1. In addition, as the temperature is raised, a hot band appears ~150 cm^{-1} below A_1. A Boltzmann plot of the intensity of this hot band vs. temperature (Figure 5) indicates it to be populating off the origin A_1. If this hot band results from the thermal excitation of the vibration corresponding to band A_2 in the excited state, then this would require the excited-state frequency (210 cm^{-1}) to be higher than the corresponding ground-state frequency (150 cm^{-1}). Due to the large number of vibrational degrees of freedom for this molecule, we do not attempt a vibrational assignment of the weaker structure between A_2 and A_3. A_3 is in the approximate

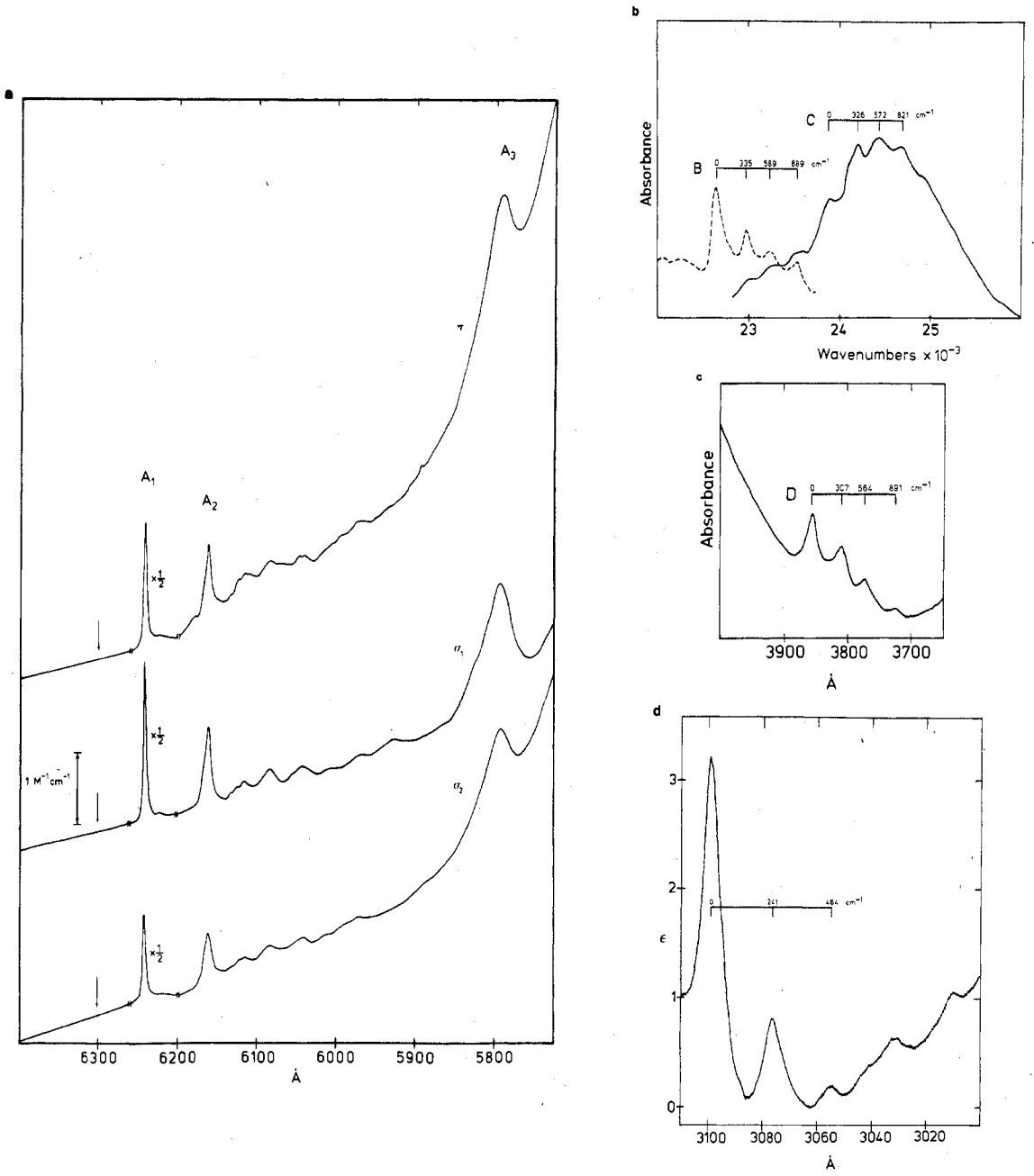

Figure 4. (a) Blow-up of low-energy region of band I showing the sharp structure of band A in π, σ_1, and σ_2 polarizations. Component A_1 occurs at 16 021 cm^{-1}, A_2 at 16 231 cm^{-1}, and A_3 at 17 268 cm^{-1}. The arrows indicate the position of the observed hot band at 15 869 cm^{-1}. (b) Blow-up of band B (dashed curve) in the X polarization and band C (solid curve) in the Z polarization. (c) Blow-up of band D in the σ_1 polarization. (d) Blow-up of the 3060-Å region in the σ_1 polarization.

energy region[9] for a carboxylate CO symmetric stretch which gives rise to a_{1g}, b_{1g}, and e_u molecular normal modes in D_{4h}. The polarization ratio of A_3 is different from that of A_1, showing that it is not totally symmetric off A_1. This, combined with its much greater intensity, points to the assignment of A_3 as a vibronic origin off the A_1 electronic origin. Thus, while most of the intensity of band A is vibronic, the pure electronic transition has some X,Y electric dipole intensity. Since the molecular site retains inversion (at least at room temperature), this state must have $E_u(D_{4h})$ symmetry. However, the lack of a low-symmetry splitting (<1 cm^{-1}) of band A_1 (the band maxima of band A_1 in the X and Y polarizations coincide) requires this state to be insensitive to the low-symmetry effects which split the broad bands I and II. A reasonable assignment, then, is that band A corresponds to an orbitally nondegenerate ungerade triplet state. Spin–orbit coupling would cause this to split into a spin–orbit E_u plus a nondegenerate level. Because the E_u level derives its degeneracy from the ± 1 spin functions,[10] it would be expected to have the required insensitivity to low-symmetry distortions. This assignment would also be consistent with the extremely low intensity of band A ($\epsilon \approx 1$ M^{-1} cm^{-1}), which is comparable to that of spin-forbidden bands in mononuclear Cr^{2+} complexes.[11]

Bands B and C (Figure 4b) overlap the more intense band I, where in Figure 3 the most intense member of band B can be seen as a sharp peak on the high-energy side. Band B is predominantly X,Y polarized, while band C is polarized along

(9) A. M. Heyns, *J. Mol. Struct.*, **11**, 93 (1972).

(10) G. F. Koster, J. O. Dimmock, R. G. Wheeler, and H. Statz, "Properties of the Thirty-Two Point Groups", MIT Press, Cambridge, Mass., 1963.

(11) W. A. Runciman and R. W. G. Syme, *Philos. Mag.*, **8**, 605 (1963).

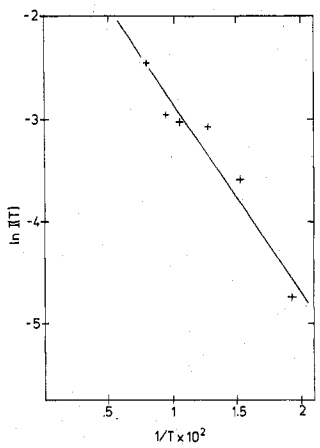

Figure 5. log plot of hot-band intensity vs. $1/T$. A least-squares fit (solid curve) to the data gives a ground-state vibrational energy $\hbar\omega = 129 \pm 25$ cm^{-1}.

the Z molecular axis. The spectra shown in Figure 4b were obtained by subtracting a least-squares Gaussian fit of band I from the digitized experimental spectrum. Band D (Figure 4c) is fairly isolated and predominantly X,Y polarized. Finally, at least two broad, weak transitions overlap the low-energy tail of band II (one predominantly Z polarized peaking at ~27 400 cm^{-1} and an X,Y polarized band peaking at ~28 500 cm^{-1}) and a sharp weak X,Y polarized transition lies on the high-energy side (Figure 4d).

Having determined that none of the sharp structure is associated with the two dominant spectral features, we proceed in the investigation of bands I and II through an analysis of their absorption band shapes and response to a variety of chemical perturbations, in order to understand these excited states within the framework of a molecular orbital picture.

Although bands I and II have similar polarizations, low-symmetry splittings, and intensities, there are large differences in their relative band shapes (Figure 3). Since the absorption band shape contains information about the nature of the excited state, the temperature dependence of the band shapes for bands I and II has been investigated to further ascertain the assignment of these transitions. In the simplest picture, the adiabatic potential surfaces (in the Born–Oppenheimer approximation) for the ground and excited states are quadratic functions of a normal coordinate Q and have equal vibrational spacings. The excited state is in general displaced by an amount ΔQ relative to the ground state in this normal coordinate. This gives rise to a low-temperature absorption band shape which consists of a series (progression) of vibronic transitions from the zeroth vibronic level of the ground state to the nth vibronic level of the excited state (Franck–Condon effect) with relative intensity given as eq 3a where S is the

$$I_n/I_0 = S^n/n! \tag{3a}$$

dimensionless Huang–Rhys parameter defined by eq 3b and

$$S = \frac{\frac{1}{2}\mu\omega_Q^2(\Delta Q)^2}{\hbar\omega_Q} \tag{3b}$$

where μ and ω_Q are the reduced mass and the vibrational frequency, respectively, for the normal coordinate Q. The intensity distribution represented by eq 3a is a Poisson distribution which, in the limit that S becomes large, is to a good approximation represented by a Gaussian distribution (semiclassical Franck–Condon principle).[12] As the temperature is increased, higher vibronic levels of the ground state ($n > 0$) will become thermally populated and new transitions can

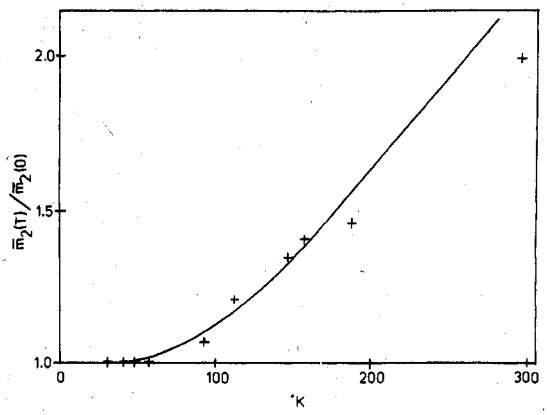

Figure 6. Plot of $\bar{m}_2(T)/\bar{m}_2(T = 0)$ as a function of temperature for band I. The solid curve corresponds to the function coth $(\hbar\omega/2kT)$ where $\hbar\omega = 228$ cm^{-1} (see Table II).

Table II. Huang–Rhys Parameters and Effective Frequencies Obtained from Least-Squares Fit to Eq 5

band	S	$\hbar\omega$
I	40.8 ± 0.8	228 ± 24
II	6.7 ± 1.6	199 ± 21

take place between these higher energy ground-state levels and levels of the excited state. The distribution of intensity at higher temperature can be characterized by its moments which are defined by eq 4 where $I(E)$ is the intensity distribution as

$$M_0 = \int I(E)\,dE \qquad m_1 = \frac{1}{M_0}\int I(E)E\,dE$$
$$\bar{m}_2 = \frac{1}{M_0}\int I(E - m_1)E^2\,dE \tag{4}$$

a function of energy (E). In particular, it has been shown[12] that the normalized second central moment ($\bar{m}_2$) is given by eq 5. For large S, where the intensity distribution is ap-

$$\bar{m}_2 = S(\hbar\omega_Q)^2 \coth(\hbar\omega_Q/2kt) \tag{5}$$

proximately Gaussian, the full width at half-maximum (fwhm) of the band can be related to $\bar{m}_2$, where

$$\bar{m}_2(\text{Gaussian}) = \frac{(\text{fwhm})^2}{8 \ln 2} \tag{6}$$

From measurements of $\bar{m}_2$ for an absorption band shape as a function of temperature, the parameters S and $\hbar\omega_Q$ can be determined by performing a least-squares fit of these data to eq 5. In general, a band shape may be composed of progressions in several normal modes having different values of S and $\hbar\omega_Q$. In this case, $\bar{m}_2$ is equal to a sum of terms like eq 5. Provided that the vibrational frequencies ($\hbar\omega_Q$) are approximately equal, the above procedure will yield[13] an effective frequency $\hbar\omega_{\text{eff}}$ and the sum of the Huang–Rhys parameters S_{eff}.

We now apply this method to the analysis of bands I and II. The temperature dependence of band I is quite dramatic and is shown in Figure 6. The results of the least-squares analysis to eq 5 for both bands is presented in Table II. Both excited states are found to be distorted in modes of similar effective frequency ($\hbar\omega \approx 200$ cm^{-1}). Vibrational energy spacings in the 200–300-cm^{-1} range are also observed in the structure associated with the weak absorption bands (Figure 4), and band A, which is not complicated by overlap, exhibits a 210-cm^{-1} progression in absorption. Since it is the Cr–Cr stretch which is expected to be the dominant progressional

(12) M. Lax, *J. Chem. Phys.*, **20**, 1752 (1952).

(13) D. B. Fitchen in "Physics of Color Centers", W. B. Fowler, Ed., Academic Press, New York, 1968, p 293.

Table III. Energy Changes[a] (and Associated S Values) for Transitions to E(D_{4h}) Symmetry Excited States

orbital transition	excited-state symm (D_{4h})	δE[b]	S
$\delta \rightarrow \pi^*$	E_g	2310	40.8
$\pi \rightarrow \delta^*$	E_g	2310	
$\pi \rightarrow \sigma^*$	E_g	5487	230
$\pi \rightarrow 4b_{2u}$	E_g	2888	64
$\pi \rightarrow 5b_{1g}$	E_u	2310	41
$\sigma \rightarrow \pi^*$	E_g	5198	207
$1a_{1u}(np_\pi) \rightarrow \pi^*$	E_u	1011	7.8

[a] $\delta Q = 0.16$ Å. [b] Energies in cm^{-1}.

mode in this molecule by analogy to $Mo_2(CH_3CO_2)_4$,[2d,e] we obtain the approximate vibrational frequency of this mode as 200–250 cm^{-1}. This analysis (Table II) also shows that the excited states associated with bands I and II have very different S parameters and, therefore, very different excited-state distortions. Taking these excited-state distortions to occur primarily along a coordinate which can be associated with the Cr–Cr bond length, then the change in equilibrium bond length upon excitation is expected to be much greater in state I than in state II.

These Huang–Rhys parameters can now be utilized for spectroscopic assignment. Since the adiabatic potential surfaces are assumed to be quadratic, we have (for the excited electronic state a) expression 7a. The results of the moment

$$\left\langle a\left|\left(\frac{\partial V}{\partial Q}\right)_0\right|a\right\rangle = \mu\omega_a^2(\Delta Q)_a$$

$$\frac{\left(\left\langle a\left|\left(\frac{\partial V}{\partial Q}\right)_0\right|a\right\rangle\right)^2}{2\hbar\mu\omega_a^3} = \frac{\frac{1}{2}\mu\omega_a^2(\Delta Q)_a^2}{\hbar\omega_a} = S_a \qquad (7a)$$

analysis for bands I and II show $\hbar\omega_I \approx \hbar\omega_{II}$. Assuming the same dominant distorting mode for these two transitions then gives eq 7b. The quantities $\langle I, II|(\partial V/\partial Q)_0|I, II\rangle$ represent

$$\frac{S_I}{S_{II}} = \left[\frac{\left\langle I\left|\left(\frac{\partial V}{\partial Q}\right)_0\right|I\right\rangle}{\left\langle II\left|\left(\frac{\partial V}{\partial Q}\right)_0\right|II\right\rangle}\right]^2 \qquad (7b)$$

the change in electronic energy of state I, II for a small change along normal coordinate Q in the vicinity of the ground-state equilibrium value of Q. If Q is the Cr–Cr stretching mode, then a change in bond length, δQ, will produce a change in energy, δE, for states I and II and the quantity $(\delta E/\delta Q)_{I,II}$ will be approximately equal to $\langle I, II|(\partial V/\partial Q)_0|I, II\rangle$. Cotton et al.[1e] have calculated the SCF–Xα 1e molecular orbital energies for the related molecule $Cr_2(HCO_2)_4$ at two different Cr–Cr bond lengths. From this calculation, the changes in energy for transitions to E(D_{4h}) symmetry excited states can be obtained (by using orbital energy differences) and are presented in Table III (column 3). Through the use of eq 7b, we now compare the results of these calculations with the experimentally obtained S parameters for bands I and II. From the calculation, the lowest spin-allowed transitions to orbital E(D_{4h}) states are the $\delta \rightarrow \pi^*$ and $\pi \rightarrow \delta^*$ one-electron excitations. With assignment of band I ($S_I = 40.8$) as one of these two possibilities, the predicted S values for the other orbital E(D_{4h}) states can be calculated by using eq 7b and are presented in Table III (column 4). We see that the only transition consistent with band II ($S_{II} = 6.7$) is the $np_\pi \rightarrow \pi^*$ transition. This prediction is independent of whether band I is taken to be either $\delta \rightarrow \pi^*$ or $\pi \rightarrow \delta^*$, as the calculation predicts the same $(\delta E/\delta Q)$ for both excited states. It should be noted that we are using the results of the SCF–Xα calculation to obtain small changes in the relative energies of two transitions as a function of metal–metal distance rather than the absolute magnitude of these transition energies or a detailed description of the molecular wave functions.

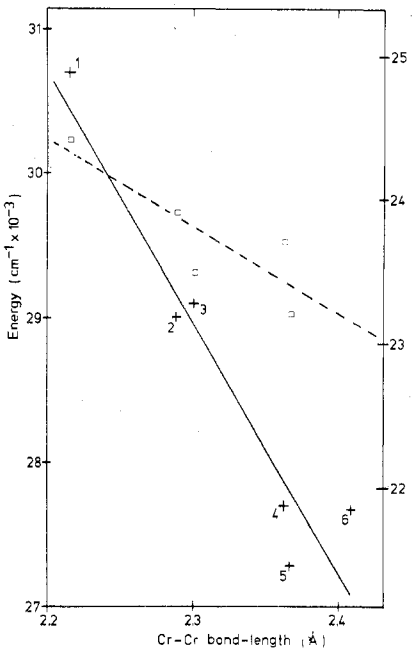

Figure 7. Plot of the energies of band I (solid curve, crosses) and band II (dashed curve, squares) as a function of Cr–Cr bond length. The solid curve goes with the energy scale to the right and the dashed curve with the scale on the left. Key: 1 = $(NH_4)_4(Cr_2(CO_3)_4(H_2O)_2)(H_2O)$; 2 = $Cr_2(CH_3CO_2)_4$; 3 = $Cr_2(CH_3CO_2)_4(CH_3CO_2H)_2$; 4 = $Cr_2(CH_3CO_2)_4(H_2O)_2$; 5 = $Cr_2(HCO_2)_4(H_2O)_2$; 6 = $Cr_2(HCO_2)_4(C_5H_5N)_2$.

Although the above treatment has made use of several approximations, its applicability may be verified experimentally. The relative shift of the band maxima (in the absorption spectrum) for a change in Cr–Cr bond length is also related to the relative values of S through relation 7b. Thus the position of the absorption band maxima for a variety of related $Cr_2(RCO_2)_4L_2$ species has been measured. This data is plotted in Figure 7. The Cr–Cr bond lengths for these species have been determined by Cotton et al.[4] The satisfactory agreement between the relative slopes (slope I/slope II = 2.6) and the square root of the relative S values ($(S_I/S_{II})^{1/2} = 2.5$) gives strong support to our previous treatment, provided that the changes in energy are primarily due to changes in the metal–metal bond length and not to ligand-related effects, as indicated by the 200–250-cm^{-1} effective vibrational frequency. Effects due to changes in axial ligands can be eliminated by noting that point 2 ($Cr_2(CH_3CO_2)_4$) and point 3 ($Cr_2(CH_3CO_2)_4(CH_3COOH)_2$) have nearly equal metal–metal bond lengths, equivalent carboxylate ligands, and very different axial ligands and yet are similar in energy. Also, only small effects are associated with changes in carboxylate ligands from a similar comparison of points 4 ($Cr_2(CH_3CO_2)_4(H_2O)_2$) and 5 ($Cr_2(HCO_2)_4(H_2O)_2$). Thus it is reasonable to attribute the changes in band maximum energy over this series primarily to changes in Cr–Cr bond length.

Discussion

In the Results, an analysis of the lowest energy transitions (band A) has allowed us to make a reasonable assignment that this band and possibly the remaining weak features in the $Cr_2(CH_3CO_2)_4(H_2O)_2$ absorption spectrum are due to electronic transitions to spin-forbidden triplet states. From this it would follow that the much more intense bands I and II are spin-allowed transitions with band I being the lowest energy transition observed of this multiplicity. From the polarization

data presented, we conclude that bands I and II must derive from orbitally degenerate (E) electronic states in the approximate D_{4h} symmetry of the molecule. By association of band I with one of the two lowest energy transitions predicted from the SCF–Xα calculations[1e] ($\delta \rightarrow \pi^*$ or $\pi \rightarrow \delta^*$), the analysis in the Results then shows that band II must be assigned as the $np_\pi \rightarrow \pi^*$ transition. This transition corresponds to an electron jump from a nonbonding π orbital localized on the carboxylate ligand into the antibonding π^* localized on the metal ions (charge transfer) and is formally allowed by the approximate D_{4h} symmetry of the molecule. This is in contrast to the $\delta \rightarrow \pi^*$ or $\pi \rightarrow \delta^*$ transitions which are g $\rightarrow$ g and hence, forbidden. The relative similarity in intensity of these two transitions (Figure 3) can be understood in the following manner. Band I, being orbitally forbidden, gains intensity through a vibronic coupling mechanism, consistent with the observed ϵ ($\approx$120 M^{-1} cm^{-1}/dimer) which is in the correct range for a vibronically allowed band. Band II, although formally allowed by the molecular symmetry, is a charge-transfer transition from an oxygen p lone-pair orbital (oriented transversely to the Cr–Cr′ axis) into an *xz* or *yz* orbital localized on the chromium. Since these two sets of orbitals are directed away from each other, orbital overlap is expected to be small and the corresponding transition intensity will be weak. This effect is similar to that found[14] for the weak $n \rightarrow \pi^*$ transitions in carbonyl spectra, where the nonbonding oxygen p orbital has a nodal plane containing the π^* molecular orbital resulting in a formal overlap of zero in the local C–O symmetry.

In regard to the assignment of band I as either $\delta \rightarrow \pi^*$ or $\pi \rightarrow \delta^*$, we recall the fact that the low-symmetry splittings for bands I and II are similar (see Figure 3). Because this splitting must come from the splitting of the e(D_{4h}) orbital involved in the transition, a consistent assignment would require band I to be the $\delta \rightarrow \pi^*$, thus explaining the similar low-symmetry effects in the two bands. This is also consistent with recent calculations[15] which would place the $\delta \rightarrow \pi^*$ transition as the lower of the two bands. As to the location of the $\pi \rightarrow \delta^*$ transition, one possibility is that its vibronic intensity is considerably less that that of the $\delta \rightarrow \pi^*$ transition which, combined with its predicted broad band shape (S = 40.8), would make it difficult to be observed in the strongly overlapped region between bands I and II, where it is calculated to lie. Alternatively, the $\pi \rightarrow \delta^*$ ($^1E_g \leftarrow {}^1A_{1g}$) transition could be at significantly higher energy, which might result from configurational interaction between the two ^1E_g states. Configurational interaction has been shown to be quite important in determining the appropriate Hartree–Fock ab initio wave function for the ground state.[1c,2h] Since the energies of the individual metal localized orbitals are quite close, it can be expected that a multiconfigurational wave function will be required to adequately describe the ^1E_g states as well. These effects are only partially included in the SCF–Xα molecular orbital method.

The weak features observed (Figure 4) in the absorption spectrum of $Cr_2(CH_3CO_2)_4(H_2O)_2$ raise some interesting questions as to their relative sharpness as compared to bands I and II. Their band shapes would indicate that the excited states associated with these transitions are relatively undistorted from the ground-state equilibrium geometry. From a simple MO picture (and the analysis in the Results), it is difficult to rationalize the undistorted geometry of these states unless they involve only nonbonding or weakly bonding orbitals such as the δ or δ^*. One possible assignment for band A, then, is the $^3A_{2u} \leftarrow {}^1A_{1g}$ ($\delta \rightarrow \delta^*$) transition. This is consistent with the requirement of an orbitally nondegenerate ungerade triplet state for band A as discussed in the Results. Since the corresponding spin singlet would be expected to be found at higher energy, the *Z*-polarized band C would then be a likely candidate for the $^1A_{2u} \leftarrow {}^1A_{1g}$ ($\delta \rightarrow \delta^*$) transition, which, although formally allowed by symmetry, would again be weak due to a small overlap of the *xy* orbitals on the two chromium centers. However, band C is broader than band A which would require the electronic–nuclear interactions in the triplet to be somewhat different from those in the singlet.

Finally, these spectral studies have allowed the ground-state Cr–Cr stretching frequency for chromous acetate dihydrate to be estimated as in the 150–250-cm^{-1} range, consistent with the weaker quadruple bond expected for chromium as compared to molybdenum carboxylates. The excited-state frequencies observed in the structured bands vary somewhat, but all are higher than the 150-cm^{-1} hot band associated with band A or the 200–230-cm^{-1} effective vibrational frequency obtained from band shape analysis of bands I and II. In other quadruply bonded complexes where excited-state frequencies are known, the metal–metal stretch shifts to lower frequency upon electronic excitation. As this increased frequency does not seem to correlate with changes in the excited-state metal–metal distance, it may indicate that the excited-state vibrational wave functions are mixed differently than in the ground state.

Acknowledgment. We thank F. A. Cotton for unpublished SCF–Xα calculational results on $Cr_2(CH_3CO_2)_4(H_2O)_2$ and useful discussions. We also acknowledge helpful discussions with H. B. Gray, W. C. Trogler, and D. S. Martin. Finally, we are grateful to S. R. Desjardins for help in the final preparation of the manuscript. This research was supported by the Cabot Solar Energy Fund.

Registry No. **1**, 31276-88-7; **2**, 15020-15-2; **3**, 15225-50-0; **4**, 14404-41-2; **5**, 60428-77-5; **6**, 64626-97-7.

(14) J. W. Sidman, *Chem. Rev.*, **58**, 689 (1958).
(15) F. A. Cotton, private communication.